Improvement of near-surface attenuation estimation

Nizare El Yadari, Delft University of Technology, Dept. of Geotechnology, Fabian Ernst and Wim Mulder, Shell International Exploration and Production*

Summary

We present a refinement of a near-surface attenuation estimation method for complex geological settings. The technique is based on visco-acoustic wave propagation modeling. We study the influence of the source wavelet and the presence of rough surface topography. Numerical simulations and measurements on field data demonstrate the improved effectiveness of the method.

Introduction

Seismic imaging of complex structures remains a challenge. Standard velocity analysis is inadequate for estimating accurate background velocity models as required for pre-stack migration and inversion. Moreover, the precise definition of a reliable macro-model is still an open question that has been addressed only in a heuristic way (Operto et al., 2000). As an alternative, full waveform inversion (Mulder and Plessix, 2006) may provide an improved earth model, but this method will only work if the starting model is sufficiently close to the correct model. This is especially true for the near surface. We need accurate modeling of both the amplitude and the phase information of all arrivals to explain the seismic data. However, existing attenuation estimation methods (Toksöz and Johnston, 1981) yield inaccurate results. To improve this situation, we developed an algorithm that uses the complete seismogram to recover the near-surface attenuation properties (El Yadari et al., 2007). This algorithm was applied to a data set recorded in the Middle East and provided an acceptable result. We estimated only the attenuation in the top layer. Here, we extend the method to multiple layers.

Outline of the method

The most common measure of attenuation is the dimensionless quality factor Q, the ratio of stored energy to dissipated energy. In the case of a layered medium, the attenuation can be included by adding an imaginary part to the velocity V_j for each layer (j = 1 to M). The modified velocity in the j^{th} layer is

$$\tilde{V}_j = V\left(1 - \frac{i}{2Q_r}\right).$$

Consequently, for (l/2Q) << 1, attenuation causes the wave amplitude to be multiplied by $e^{-\alpha x}$, where $\alpha = \omega/(2VQ)$ and x is the distance in the direction of propagation. An alternative, causal absorption involves an extra frequency-dependent term modifying the real part of the velocity. The extra term results in an expression:

$$\tilde{V}_j = V\left(1 - \frac{i}{2Q_r} - \frac{1}{\pi Q_r}\ln\left(\frac{\omega}{\omega_r}\right)\right).$$

The selection of the reference frequency ω_r and the modified quality factor Q_r is discussed in (O'Neil and Hill, 1979). We aim at estimating the attenuation in the near surface where the attenuation is strongest. Because we presented the details elsewhere (El Yadari et al., 2007), we only mention a few properties that will be used here. Full waveform tomography requires the definition of a good initial model. To develop such a starting model, refraction statics (Zanzi and Carlini, 1991) can provide a horizontally layered model with density ρ_j, depth d_j, and velocity V_j for each layer. Hence, we assume that $\boldsymbol{\rho}$, $\mathbf{d}$ and $\mathbf{V}$ (vectors with a length M equal to the number of layers) are known and we only want to determine the attenuation parameters, denoted by the vector $\mathbf{Q}$. The subsurface model in question is assumed to be a layered medium where Q_j is constant in each layer. A set of N models characterized by $\mathbf{Q^k} = \{Q_1^k, Q_2^k, ..., Q_M^k\}$, k = 1 to N, is defined. Among all these models, we want to find the most likely one. A 2D visco-acoustic finite difference frequency-domain modeling code is subsequently used to simulate the full wavefield for each one of the N subsurface models. The synthetic seismogram resulting from each simulation is then compared to the observed one, leading to the desired attenuation model, denoted by $\mathbf{Q}^{\mathbf{Measured}}$. The comparison step consists of using the travel time for refracted and reflected waves to pick amplitudes from each synthetic and observed seismogram. Then, the most likely $\mathbf{Q}^{\mathbf{Measured}}$ is given by the minimum value of a specific error measure.

Error measure

We present a preliminary study of the relationship between pairs of Q_j. To describe this relationship, we define an error criterion that measures the difference between the picked amplitudes:

$$E\left(\mathbf{Q}^k\right) = \frac{1}{M}\sum_{n=\text{Layers}} \alpha_n E_n\left(\mathbf{Q}_n^k\right),$$

where α_n is the weight assigned to the n^{th} layer and

$$\sum_{n=\text{Layers}} \alpha_n = 1.$$

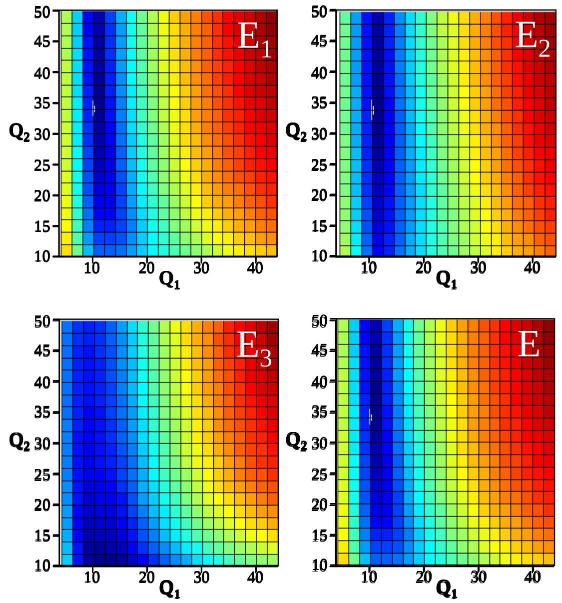

Figure 1: Errors as a function of Q_1 and Q_2 for fixed Q_3 and Q_4, calculated for the 1st layer (E_1), 2d layer (E_2), 3rd layer (E_3) and their total sum (E).

$E_n(Q_n^k)$ is the error corresponding to the n^{th} layer that we used earlier (El Yadari et al., 2007). In the current example, all synthetic seismograms are calculated for a range of frequencies between 8 and 20 Hz. We still use a 4-layer subsurface model with the same features as the one in (El Yadari et al., 2007) and the same source and receiver positions.

To explain the concept of the improved method, we only allow Q_1 and Q_2 to vary and assume fixed $Q_3 = 40$ and $Q_4 = 100$. We computed 441 synthetic seismograms for $Q_1 = 4, 6,\ldots, 44$ and $Q_2 = 10, 12,\ldots, 50$. These 441 seismograms were then successively compared with what we call the observed seismogram. This was either the same as the real seismogram used in (El Yadari et al., 2007) or a synthetic one. Use of the latter amounts to an inverse crime but allows for validation. For each comparison, we present an image of the error criterion. All errors were measured with $\alpha_1 = \alpha_2 = \alpha_3$ and $\alpha_4 = 0$. Figure 1 shows the contribution of E_1, E_2 and E_3 to the total error E for the synthetic test. We can observe that Q_1 is better resolved than Q_2.

Influence of the source wavelet

Because our method involves frequency-dependent wave propagation, the spectrum of the source wavelet is important. We therefore studied the influence of the dominant frequency band and of the shape of the estimated wavelet. We used the two different estimated wavelets shown in Fig. 2 to transform the synthetic seismogram computed with the frequency-domain code to the time domain. Both wavelets were used for the 441 synthetic

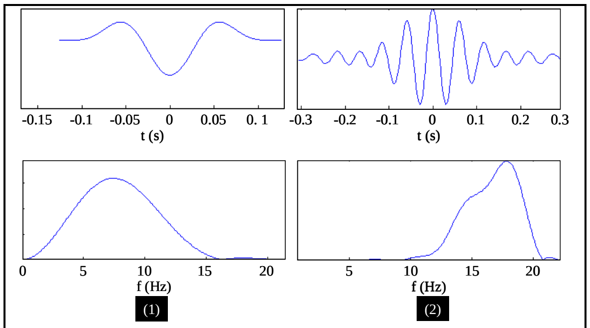

Figure 2: Estimated wavelets used to convert seismogram to time domain.

seismograms. Note that the wavelet on the left-hand side, labeled by (1), has a spectrum that does not coincide with the range of frequencies used for modeling. The spectrum of the second wavelet, labeled by (2), does coincide. The wavelet (1) is intentionally chosen wrong. The other one is estimated from the observed seismogram.

Dominant frequency band

Figure 3 shows two error images. The left panel corresponds to the use of wavelet (1), the right one to wavelet (2). The observed seismogram is the synthetic one calculated for $Q_1 = 10$ and $Q_2 = 34$. In each case, it is transformed with the corresponding wavelet. The comparison between both images shows a similar behavior of the error criterion. As a result, there is no dependency of the dominant frequency band.

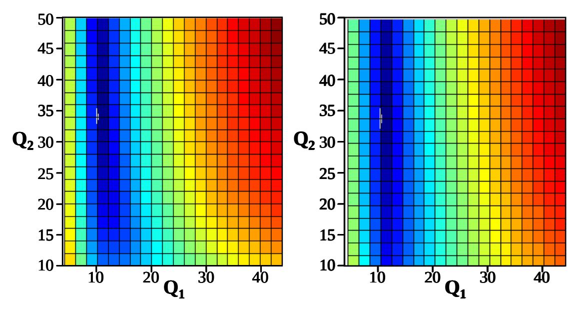

Figure 3: Error images showing the influence of the dominant frequency band.

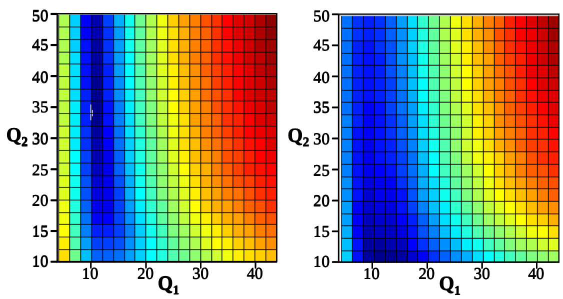

Figure 4: Error images representative of the influence of the estimated wavelet.

Estimated wavelet

In order to evaluate the effect of the inaccuracy of the estimated wavelet, the 441 seismograms obtained with wavelet (1) were compared with the synthetic reference data calculated with $Q_1 = 10$ and $Q_2 = 34$, transformed to the time domain with wavelet (2). The resulting image is displayed in Fig. 4 on the right-hand side and compared to the one obtained for the correct wavelet (left panel in Fig. 4). The comparison shows how strong the effect of the estimated wavelet can be. This can be easily explained by realizing how the first-arrival travel times were picked. We picked the maximum-amplitude peak nearest to the one predicted by the travel-time formulas. Consequently, a strong change of the wavelet will affect the picked amplitude as well as the corresponding error criterion. As an improvement, we may consider the energy inside a window around the peak instead of the amplitude, but this option was not considered here.

Topography

Because of the presence of rough topography, we must include elevation statics when calculating the travel times of the first arrivals. In (El Yadari et al., 2007), we presented formulas for travel times, denoted by $t_n^{Refr}(h)$ and $t_n^{Refl}(h)$, of a ray refracted or reflected along the top surface of the nth layer given a source-receiver distance h for the case of a flat surface. Here, we make an extension to the case of elevated sources and receivers (see Fig. 5). Then,

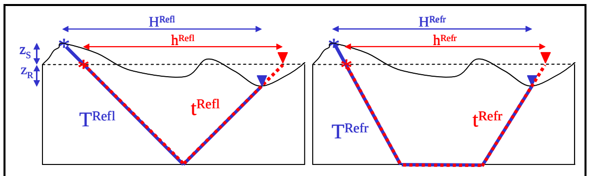

Figure 5: Schematic overview of a ray reflected or refracted along the top surface of a layer.

$$T_n^{Refr/Refl} = t_n^{Refr/Refl}(H^{Refr/Refl}) - \Delta t^{Refr/Refl},$$

with

$$H^{Refr} = \frac{z_r + z_s}{\sqrt{\left(V_2/V_1\right)^2 - 1}} + h^{Refr},$$

and

$$H^{Refl} = \frac{h^{Refl}}{1 - \dfrac{z_r + z_s}{2d_1}}.$$

Here z_s and z_r denote the source and the receiver elevations, respectively. V_1 and V_2 are the velocities of the 1st and 2nd layers and d_1 is the thickness of the 1st layer. Elevation corrections for refracted and reflected travel times are given by

$$\Delta t^{Refr} = \frac{z_s + z_r}{V_1} \frac{1}{\sqrt{1 - \left(V_1/V_2\right)^2}},$$

and

$$\Delta t^{Refl} = \frac{z_s + z_r}{V_1} \sqrt{1 + \left(H^{Refl}/2d_1\right)^2}.$$

As an example, Figure 6 shows the source and receiver elevations for the real data set used in (El Yadari et al., 2007). The effects of elevation statics correction on the picked travel times are displayed in Fig. 7. The latter are shown from the top to the bottom of the figure as curves corresponding to the refraction and reflection travel times calculated for the 1st, 2nd, and 3rd layer. Note that the curves without static corrections are shown on the left-hand side.

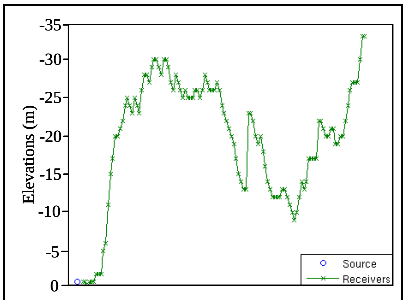

Figure 6: Elevations of the source and the receivers.

Field data

We want to improve the application of our near-surface attenuation estimation method to the field data. The application to synthetic data has demonstrated the need for a correct estimate of the wavelet. To determine the wavelet

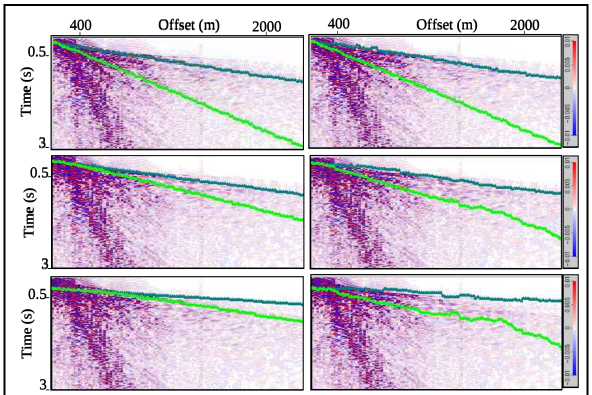

Figure 7: Refraction (blue line) and reflection (green line) travel times curves picked on traces from real data. The curves on the left were obtained without and on the right with static corrections.

for the field data, a near-offset trace was zero-phased. We only kept the part of its spectrum between 8 and 20 Hz. The resulting wavelet is the one marked by (2) in Fig. 2. Note that we corrected the travel times for elevation statics in the observed seismogram, but did not include topography nor elevation statics in the finite-difference modeling. The amplitudes obtained from the curves in Fig. 7 were inserted into the error criterion in order to measure how well Q_1, Q_2 and Q_3 explain the data. As our finite-difference code is 2-D and wave propagation for real data occurs in a 3-D medium, a rather crude 2-D to 3-D conversion was performed (Crase et al., 1990). The amplitudes used by the error criterion were normalized by their maximum over the data. Figure 8 show the errors for the case without elevation static on the left and with on the right. The results show a reasonably smooth behavior of both images. Note the enhanced resolution of the image obtained with elevation statics. The minimum value obtained for Q_1 is equal to 22. It agrees with typical regional values inferred from shear-wave Q measurements and the ratio between shear-wave and compressional-wave attenuation given in (Mokhtar et al., 1988). However, we appear to obtain a value of 10 for Q_2, whereas we would expect a value equal to or larger than Q_1. One explanation could be that our subsurface model is not accurate enough. There even might not be interface between the 1st and the 2nd layer. In that case, Q_2 can be ignored and Q_3 is around 24. Another explanation is that Q_2 is about 20, implying that Q_3 is about 20 as well, judging from the right lower panel in Fig. 8.

Figure 8 suggests that optimization of the attenuation parameters in the near surface should be feasible, either deterministic or in a probabilistic sense. Layer-stripping may be the way to go: first we can determine Q_1 by analyzing the behavior of Q_1 and Q_2, as in the top row of Fig. 8, and then we can estimate Q_2 by considering Q_2 and Q_3 at the estimated Q_1, as in the second row of Fig. 8, and so on.

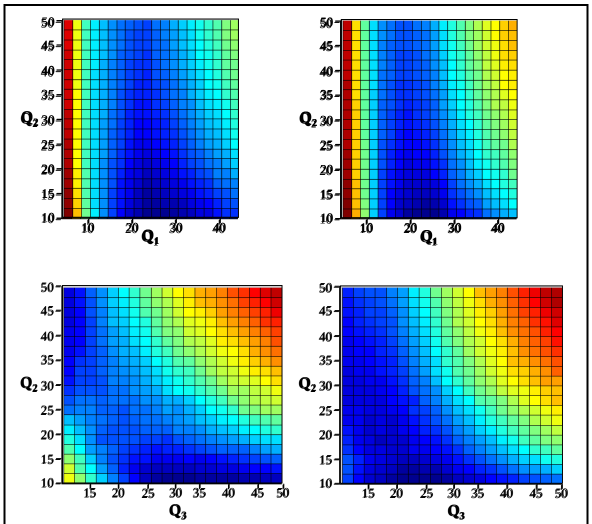

Figure 8: Error images calculated for the field data in both cases without (left) and with (right) elevation statics. The two lower panels were obtained for a fixed value of Q_1 = 22.

Conclusion

We have presented a refinement of our method to estimate near-surface attenuation using a visco-acoustic frequency-domain finite-difference modeling code. We included elevation statics in the reflection and refraction travel times used for picking amplitudes. The results showed an enhanced resolution of the image obtained with elevation statics. The wavelet should be carefully estimated. We applied the method to field data. Therefore, the estimated attenuation factors for real data should be reasonably accurate.

The next step is the use of a finite-difference code that includes topography and models the visco-elastic case. Note that here we already took the effect of geometrical spreading and the source wavelet into account.

EDITED REFERENCES

Note: This reference list is a copy-edited version of the reference list submitted by the author. Reference lists for the 2007 SEG Technical Program Expanded Abstracts have been copy edited so that references provided with the online metadata for each paper will achieve a high degree of linking to cited sources that appear on the Web.

REFERENCES

Crase, E., A. Pica, M. Noble, J. McDonald, and A. Tarantola, 1990, Robust elastic nonlinear waveform inversion: Application to real data: Geophysics, 55, 527–538.

El Yadari, N., F. Ernst, and W. A. Mulder, 2007, Near-surface attenuation estimation: 69th Conference and Exhibition, EAGE, Extended Abstracts, E039.

Mokhtar, T. A., R. B. Herrmann, and D. R. Russell, 1988, Seismic velocity and Q model for the shallow structure of the Arabian shield from short-period Rayleigh waves: Geophysics, 53, 1379–1387.

Mulder, W. A., and R. E. Plessix, 2006, Full waveform tomography and nonlinear migration: 68th Conference and Exhibition, EAGE, Extended Abstracts, A038.

O'Neil, M. E., and D. P. Hill, 1979, Causal absorption: Its effect on synthetic seismograms computed by the reflectivity method: Bulletin of the Seismological Society of America, 69, 17–25.

Operto, S., S. Xu, and G. Lambare, 2000, Can we quantitatively image complex models with rays? Geophysics, 65, 1223–1238.

Toksöz, M., and D. Johnston, 1981. Seismic wave attenuation: SEG.

Zanzi, L., and A. Carlini, 1991, Refraction statics in the wavenumber domain: Geophysics, 56, 1661–1670.